Spin alignment and resonance behavior in the $^{24}Mg+^{24}Mg$ system

A. H. Wuosmaa,* R. W. Zurmühle, P. H. Kutt, S. F. Pate,† and S. Saini‡
Physics Department, University of Pennsylvania, Philadelphia, Pennsylvania 19104

M. L. Halbert and D. C. Hensley
Oak Ridge National Laboratory, Oak Ridge, Tennessee 37830
(Received 8 January 1990)

We have performed detailed particle-γ and particle-γ-γ angular correlation measurements for two strong resonances observed in the elastic and inelastic scattering of $^{24}Mg+^{24}Mg$. These data provide us with spectroscopic information relatively uncontaminated by nonresonant amplitudes, and allow spin assignments of $J^{\pi}=36^{+}$ for two resonances at $E_{c.m.}=45.70$ and 46.65 MeV. The angular correlation data for the mutual 2^{+} inelastic scattering channel suggest a dominant decay l value of $l=34$ for both resonances. Correlated spin alignment data for this channel confirm our expectations for the relationship between angular momentum coupling and spin alignment for these resonances. The relatively high spin values suggest a resonance configuration in which the two ^{24}Mg nuclei interact pole-to-pole, allowing the system to sustain a large amount of angular momentum. The pole-to-pole grazing picture is supported by the results of model calculations of the $^{24}Mg+^{24}Mg\rightarrow^{48}Cr$ system.

I. INTRODUCTION

For many years the question of resonances in heavy-ion scattering has generated great interest. The observation of intermediate-width structure in the excitation functions of elastic $^{12}C+^{12}C$ and $^{12}C+^{16}O$ was attributed to the formation of molecular configurations in these two heavy-ion systems.[1-3] These resonances have been studied extensively, and their properties are well documented and catalogued.

More recently, pronounced resonant behavior has been observed in excitation-function data for the elastic and inelastic scattering of two *sd* shell nuclei. Betts *et al.* reported intermediate width[4] and narrow structure[5] in excitation functions for the scattering of $^{28}Si+^{28}Si$. Two other α-particle systems, $^{24}Mg+^{24}Mg$ and $^{24}Mg+^{28}Si$, also exhibit strong resonance behavior.[6,7] In the case of $^{24}Mg+^{24}Mg$, these states possess weak but measurable decay branches to the mass-asymmetric exit channel $^{20}Ne+^{28}Si$.[8] The resonances in these systems have several common features. For instance, in each case the excitation-function peaks lie at energies between 1.6 and 2 times the Coulomb barrier energy, and are strongly correlated in energy between the elastic and several inelastic scattering channels. The most narrow states have widths on the order of 100–150 keV FWHM, suggesting the formation of a long-lived quasimolecular complex. Also, indications are that these resonances possess very high spin, either at or near the value of the grazing angular momentum for these systems.[4-7]

The most striking example of narrow resonance behavior lies in the $^{24}Mg+^{24}Mg$ system. Figure 1 shows excitation-function data for $^{24}Mg+^{24}Mg$ elastic and inelastic scattering obtained from Refs. 6 and 9. Several resonancelike structures appear between center-of-mass energies of 42–56 MeV, corresponding to an excitation energy range of from 56 to 70 MeV in the composite system ^{48}Cr. Despite these very high excitation energies, the observed resonances are quite narrow; states in the neighborhood of $E_{c.m.}=46$ MeV have widths of only 120–200 keV. Elastic-scattering angular-distribution measurements[6,10] suggest spins near $34-36\hbar$ for the structures seen near $E_{c.m.}=46$ MeV. These angular momenta are higher, by about $2-4\hbar$, than the calculated values of the grazing angular momentum at these energies.

The systematic behavior of these resonances remains a puzzle. To date, this type of narrow structure has only been observed in the three α-particle systems noted above: $^{28}Si+^{28}Si$, $^{24}Mg+^{24}Mg$, and $^{24}Mg+^{28}Si$. The addition of one or two neutrons to either the target, the projectile, or both, causes the resonance peaks to disappear completely. This lack of narrow structure was demonstrated[11] in studies of elastic and inelastic scattering of $^{28}Si+^{29}Si$, $^{28}Si+^{30}Si$, and $^{30}Si+^{30}Si$. Even more surprising were excitation-function data[12] from another symmetric α-particle system, $^{32}S+^{32}S$. These data displayed no resonancelike features whatsoever. Bilwes *et al.*[13] reported finding no statistically significant intermediate width structure in another α-particle system, $^{28}Si+^{32}S$. The excitation functions obtained in Ref. 13 were measured in rather wide steps, however, and might not possess sufficient resolution to be sensitive to narrow structure on the order of $\Gamma\sim100-200$ keV.

Descriptions of resonance behavior in terms of reaction models usually employed to describe resonances in lighter systems, such as the band-crossing model,[14] the double-resonance model,[15] a coupled-channels approach,[16] and the Austern-Blair model,[17] have not provided a microscopic description of the nature of these narrow structures. Perhaps more promising is the suggestion that these resonances might correspond to fissioning high spin shape isomers in the composite system.[5] This description

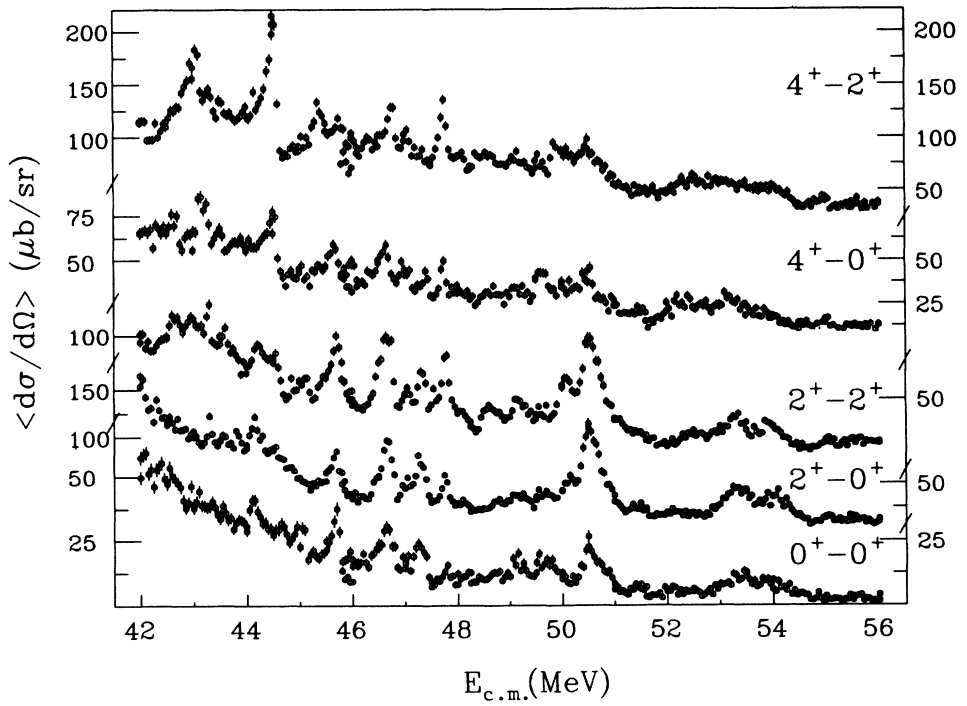

FIG. 1. Excitation-function data for $^{24}Mg+^{24}Mg$ scattering from Zurmühle *et al.* (Refs. 6 and 9) averaged over $66° \leq \theta_{c.m.} \leq 93°$.

could be particularly attractive in light of the recent discovery of superdeformed rotational bands at high spin in many nuclei in the rare-earth region.[18–21] The study of resonance behavior in the $A \sim 50$ mass region presents an opportunity to study much lighter nuclei at the extreme conditions of very high spin and excitation energy.

In the present work we have applied particle-γ-ray angular correlation techniques to the study of resonances in the $^{24}Mg+^{24}Mg$ system. Correlation and spin-alignment measurements have yielded a great deal of new insight into resonance behavior in lighter systems, such as $^{12}C+^{12}C$ (Refs. 22–25) and $^{12}C+^{16}O$.[26] In $^{24}Mg+^{24}Mg$, these measurements can provide us with clean spectroscopic information about the angular momenta involved in these resonances, and allow us to make unambiguous spin assignments for some of the observed peaks.[27] Also, these data can provide us with details of the reaction mechanism, possibly giving clues to the underlying nature of these rather curious states.

II. EXPERIMENT AND DATA ACQUISITION

We performed our γ-ray angular correlation and angular-distribution measurements using the Holifield Heavy Ion Research Facility Spin Spectrometer.[28] This device is a multidetector NaI spectrometer comprised of 70 NaI γ-ray detectors, with a total solid angle of 91.4% of 4π. The 4π coverage of the Spin Spectrometer allows for the detection of γ rays from weak reaction channels with high efficiency. In addition, the close geometry of the Spin Spectrometer permits compensation for Compton scattering and pair production in individual crystals, thus improving γ-ray peak shapes and photopeak efficiency.

The heavy-ion reaction products were detected using a recoil coincidence setup consisting of two large-area, silicon surface barrier detectors. The defining detector in the recoil coincidence setup was positioned at $\theta_{lab}=50°$, and subtended an angular range of $\Delta\theta_{lab}=13.6°$. The recoil detector was centered at 40° and had an opening angle of 18.0°. For elastic scattering, the recoil coincidence efficiency of this setup is near 95%. For inelastic scattering, the recoil efficiency falls roughly linearly with Q value, going to 0% at approximately $Q=-18.0$ MeV. In addition to the heavy-ion detectors, two small monitor detectors were placed at $\pm 10°$ to measure forward-angle elastic scattering for normalization purposes.

For particle identification, we used fast timing circuits to measure the time-of-flight difference (ΔTOF) between the reaction fragments.[7] Our defining and recoil detectors were located 8 and 6 cm from the target, respectively. At these distances, we required timing resolution on the order of 300–400 ps FWHM in order to separate adjacent α-particle reaction channels. Previous measurements[8] have shown that at low Q values inelastic scattering dominates the $^{24}Mg+^{24}Mg$ reaction cross section. The remainder of the cross section arises from the one and two α-particle transfer reactions leading to the $^{20}Ne+^{28}Si$ and $^{16}O+^{32}S$ final states, respectively. Figure 2 shows a two-dimensional particle identification spectrum, with the energy in one heavy-ion detector plotted versus the measured ΔTOF for a narrow range of Q value. Groups corresponding to the $^{24}Mg+^{24}Mg$, $^{20}Ne+^{28}Si$, and $^{16}O+^{32}S$ final states are clearly visible. We can obtain an indication of the relative strength of

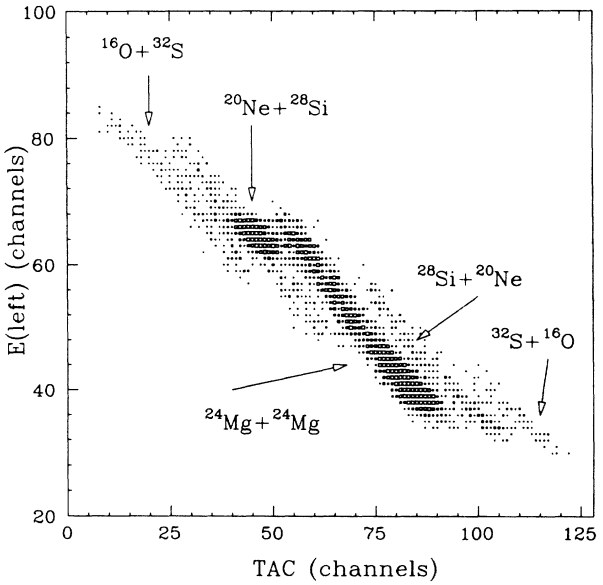

FIG. 2. Two-dimensional time-of-flight particle identification spectrum, gated on events with $-3.5 \geq Q \geq -4.5$ MeV.

the different reaction channels by straightening the different mass groups and projecting them down upon the time axis. The ΔTOF spectrum in Fig. 3 is the result of such a procedure, and clearly reflects the dominance of the $^{24}Mg+^{24}Mg$ inelastic-scattering channel. The bar in Fig. 3 corresponds to a ΔTOF of 1 ns.

The targets used in the experiment consisted of 15 $\mu g/cm^2$ of ^{24}Mg evaporated on 10 $\mu g/cm^2$ ^{12}C backings. These were bombarded with a 25 pnA ^{24}Mg beam from the 25 MV HHIRF Tandem Accelerator. Particle-γ-ray angular correlation data averaged over the scattering angle were obtained in $\Delta E_{c.m.}=100$ keV steps from $E_{c.m.}=45.45$ to 45.85 MeV, as well as

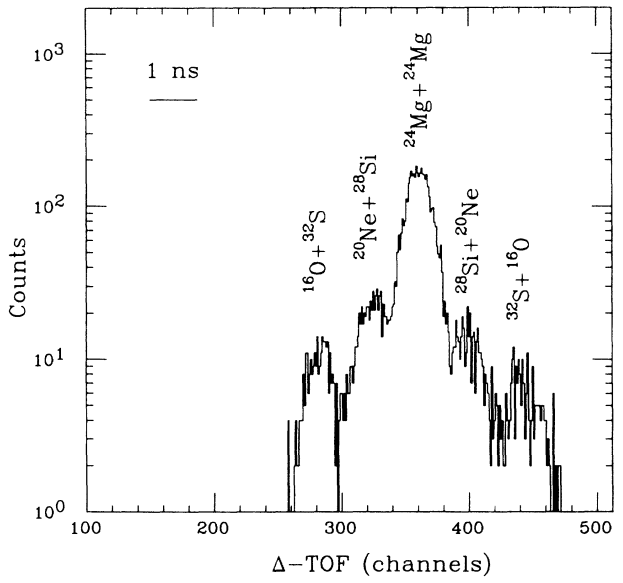

FIG. 3. ΔTOF spectrum derived by projecting the two-dimensional display in Fig. 2, showing the relative contributions of different reaction channels. The vertical axis is logarithmic.

$E_{c.m.}=46.45-46.95$ MeV. These ranges correspond to the regions of two strong, well-isolated resonances observed in $^{24}Mg+^{24}Mg$ inelastic scattering. At two energies, $E_{c.m.}=45.70$ and 45.95 MeV, we obtained statistics sufficient to study the particle angular-distribution properties of the γ-ray angular correlations. We chose the $E_{c.m.}=45.70$ MeV peak for detailed study, for, among the observed resonances, it is the structure most clearly separated from other nearby peaks. Energy signals from the two heavy-ion detectors, a time-to-amplitude converter (TAC) signal measuring the ΔTOF between the reaction fragments, as well as pulse height, timing, and identification information for each γ-ray detector that fired were recorded event by event onto magnetic tape.

III. DATA REDUCTION

The event-mode data were reduced and analyzed using a Motorola 68000 based multiple-processor array in conjunction with PDP 11/50 and MicroVAX computers.[29,30] Energy signals from the two heavy-ion detectors were first gain matched, then added together to generate Q-value spectra. Particle identification gates were then applied to the data to separate the $^{24}Mg+^{24}Mg$ exit channel from the one and two α-particle transfer channels. Figure 4 contains Q-value spectra for the $^{24}Mg(^{24}Mg,^{24}Mg)^{24}Mg$, $^{24}Mg(^{24}Mg,^{20}Ne)^{28}Si$, and $^{24}Mg(^{24}Mg,^{16}O)^{32}S$ reactions. Several low-lying excitations in each mass partition are clearly resolved. The peak identifications in Fig. 4 are based on the measured Q value, as well as γ-ray multiplicity data obtained from the Spin Spectrometer. The peaks labeled 0^+-0^+,

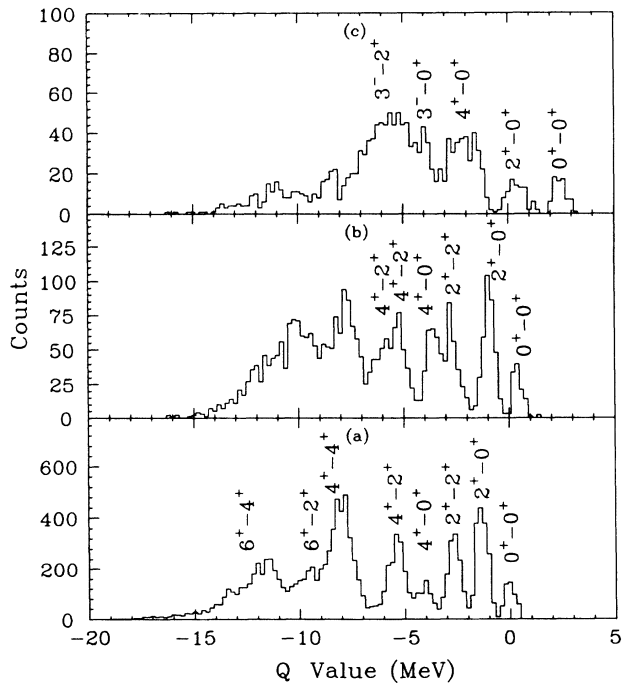

FIG. 4. Q-value spectra for the (a) $^{24}Mg(^{24}Mg,^{24}Mg)^{24}Mg$, (b) $^{24}Mg(^{24}Mg,^{20}Ne)^{28}Si$, and (c) $^{24}Mg(^{24}Mg,^{16}O)^{32}S$ reactions at $E_{c.m.}=45.45$ MeV. The excitations labeled in (a) correspond to those in Fig. 1.

2^+-0^+, 2^+-2^+, 4^+-0^+, and 4^+-2^+ in the $^{24}Mg+^{24}Mg$ data in Fig. 4(a) correspond to the excitations represented in Fig. 1. Gates on the appropriate excitation energy were then applied to the γ-ray information. After mass identification of the final-state reaction fragments, their scattering angles were derived from the energy signals in the heavy-ion detectors. Signals from each γ-ray detector were gain matched using data from ^{88}Y and Pu-Be calibration sources. We compensated for Compton scattering and pair production in the NaI crystals by using nearest-neighbor detectors to detect secondary radiation. Pulse height in nearest-neighbor crystals from Compton or pair events could then be added back into the signal from the original γ ray.

To extract the magnetic-substate population information from the γ-ray angular correlation, we begin by considering the correlation in terms of a density-matrix formalism.[27,31] The γ-ray angular correlation may be written as[31]

$$W(\theta_\gamma,\phi_\gamma)=\sum_{mm'}\rho_{mm'}F^J_{mm'}(\theta_\gamma)e^{i(m-m')\phi_\gamma}\ . \quad (1)$$

The density-matrix elements $\rho_{mm'}$ are given by

$$\rho_{mm'}=a_m a_{m'}e^{i(\delta_m-\delta_{m'})}\ ,$$

where $a_m e^{i\delta_m}$ is the reaction amplitude for a given value of m. The quantities $F^J_{mm'}$ are functions of the γ-ray polar angle, as described, for instance, by Rybicki, Tamura, and Satchler.[31]

The cylindrical symmetry of the spin spectrometer allows us to average our data over the azimuthal angle ϕ_γ. In this case, the off-diagonal contributions to the angular correlation vanish, and the resulting γ-ray angular distribution is given by

$$W(\theta_\gamma)=\sum_m P_m W_m(\theta_\gamma)\ . \quad (2)$$

The quantities $W_m(\theta_\gamma)$ simply represent the γ-ray angular-distribution functions for a pure Δm transition, and are the same as those derived by Rose and Brink.[32] The magnetic-substate population parameters P_m are then the diagonal elements of the density matrix ρ, given by $P_m=\rho_{mm}=|a_m|^2$. We obtain the cross section for a give magnetic substate m from the simple expression $\sigma_m=P_m\times\sigma$.

In the case of mutual inelastic scattering, where now two γ rays are present, we can use a similar expression to fit the correlated γ-ray angular distribution, $W(\theta_{\gamma 1},\theta_{\gamma 2})$. After the averaging of the two azimuthal angles, the correlated γ-ray angular distribution is given by[21,27]

$$W(\theta_{\gamma 1},\theta_{\gamma 2})=\sum_{m_1,m_2}P_{m_1,m_2}W_{m_1}(\theta_{\gamma 1})W_{m_2}(\theta_{\gamma 2})\ . \quad (3)$$

The quantities P_{m_1,m_2} represent correlated magnetic-substate population parameters. The correlated substate cross section is then defined by $\sigma_{m_1,m_2}=P_{m_1,m_2}\times\sigma$. The 4π geometry of the spin spectrometer also allows us to treat the γ-ray data in any coordinate system we choose. In particular, we wish to obtain substate population data in the coordinate systems with the quantization axes chosen to lie along the beam, and along the normal to the scattering plane, which can provide us with information about the angular momenta contributing to the reaction, and about the reaction mechanism, respectively.

IV. RESULTS AND ANALYSIS

A. General remarks

In this section we present the results of our measurements for the elastic, single, and mutual 2^+ inelastic-scattering channels. One aim of the analysis is to obtain model-independent determinations of the spins of the resonances that we studied. We begin by discussing our results for elastic scattering, then turn to the γ-ray correlation data for single and mutual inelastic 2^+ scattering. Combined, all of these results provide us with a comprehensive description of the reaction mechanism through which these resonances are populated. We will also briefly examine alignment data for some more highly excited states in $^{24}Mg+^{24}Mg$ scattering, as well as for the α-transfer reaction leading to the nonsymmetric $^{20}Ne+^{28}Si$ channel.

B. Elastic scattering

Figure 5 shows excitation-function data for $^{24}Mg+^{24}Mg$ elastic scattering from Zurmühle *et al.*[6,9] over the energy range of the two resonances we studied. Of the total on-resonance cross section of 38 μb/sr for the peak at $E_{c.m.}=45.70$ MeV, more than half can be attributed to the background. This result implies that in order to determine resonance spins from elastic-scattering angular distributions, one must be able to provide a detailed description of the processes contributing to the background.

Under the assumption of no background, the resonance angular distribution is given simply by

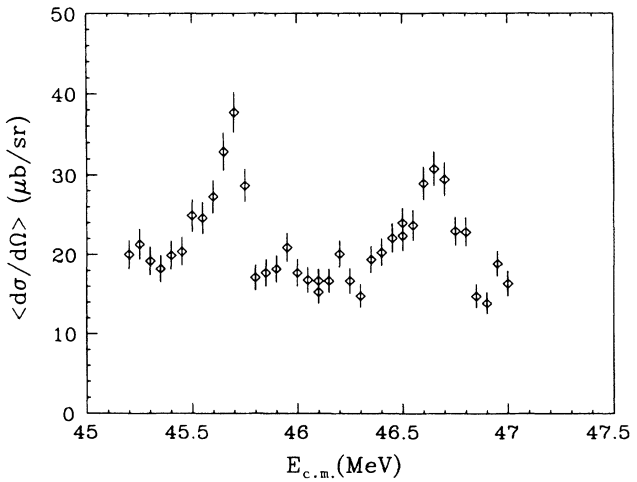

FIG. 5. Elastic-scattering excitation-function data from Zurmühle *et al.* (Ref. 6) averaged over $66°\leq\theta_{c.m.}\leq 93°$.

$$\sigma(\theta_{\text{c.m.}}) \propto |P_l(\cos\theta_{\text{c.m.}})|^2 ,$$

where l corresponds to the resonance angular momentum. Figure 6 contains on-resonance angular-distribution data for the two peaks we studied, at $E_{\text{c.m.}}=45.70$ and 46.65 MeV. Superposed over the data are curves corresponding to squared Legendre polynomials of order 34 (dashed curve) and order 36 (solid curve). Both curves give a reasonably good account of the data, with the $l=34$ curve perhaps fitting slightly better. It is still, however, quite difficult to discern from such a comparison which angular momentum corresponds to the resonance spin. One approach is to fit the angle and energy dependence of the elastic scattering cross section to an expression of the form

$$\sigma(E_{\text{c.m.}},\theta_{\text{c.m.}}) \propto \left| \sum_l A_l(E_{\text{c.m.}}) P_l(\cos\theta_{\text{c.m.}}) \right|^2 , \quad (4)$$

in hopes of determining which reaction amplitude $A_l(E_{\text{c.m.}})$ displays characteristic resonance behavior. The large amount of background and small angular range make this procedure extremely difficult, however, and the results are quite often ambiguous as to which l corresponds to the resonance spin.

In order to reduce somewhat the number of variable parameters and the ambiguity of the fit results, one could attempt to model the background, and generate nonresonance $A_l(E_{\text{c.m.}})$'s from, for instance, an optical-model calculation. Figure 7 contains off-resonance elastic-scattering angular-distribution data, obtained at energies of $E_{\text{c.m.}}=45.95$ and 46.85 MeV. Also plotted in Fig. 7 are the results of some simple optical-model calculations for the direct potential scattering background. The optical-model parameters used in this calculation were obtained from Betts[32] from fits to forward-angle elastic-scattering data and are listed in Table I. As expected, the optical-model prediction varies only slightly between the two energies, whereas the shapes of the two measured angular distributions are quite different. This result implies that the composition of the background is more complicated than that which can be described by this simple calculation, and that the contribution of background amplitudes to the on-resonance cross section will be very difficult to determine. In order to make reliable spin assignments, we must consider data less sensitive to the nonresonant scattering amplitudes. For these reasons, we now turn our attention to our particle-γ angular correlation data for ^{24}Mg+^{24}Mg inelastic scattering.

C. 2^+-0^+ excitation

Figure 8 displays magnetic-substate excitation-function data for single inelastic scattering to the 2^+ state at 1.37 MeV in ^{24}Mg. Here, the quantization axis is chosen to lie along the beam. The cross section for the $m=0$ substate shows very prominent resonance structure, with a peak-to-background ratio of approximately three to one. The $|m|=1$ substate contains somewhat weaker structure, and the $|m|=2$ substate excitation function is essentially flat. These data suggest that the $m=0$ substate will yield information about the resonance that is relatively uncontaminated by background processes.

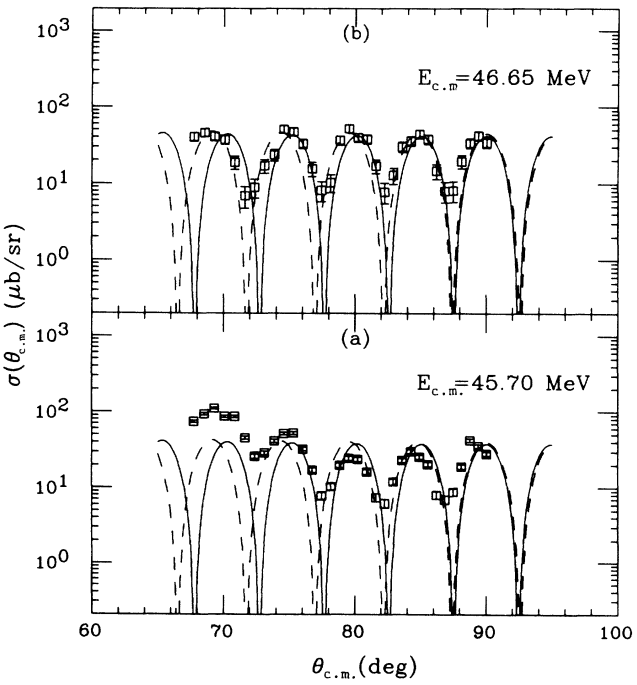

FIG. 6. On-resonance elastic-scattering angular-distribution data for (a) $E_{\text{c.m.}}=45.70$ MeV and (b) $E_{\text{c.m.}}=46.65$ MeV. The curves are squared Legendre polynomials of order 34 (dashed curve) and order 36 (solid curve).

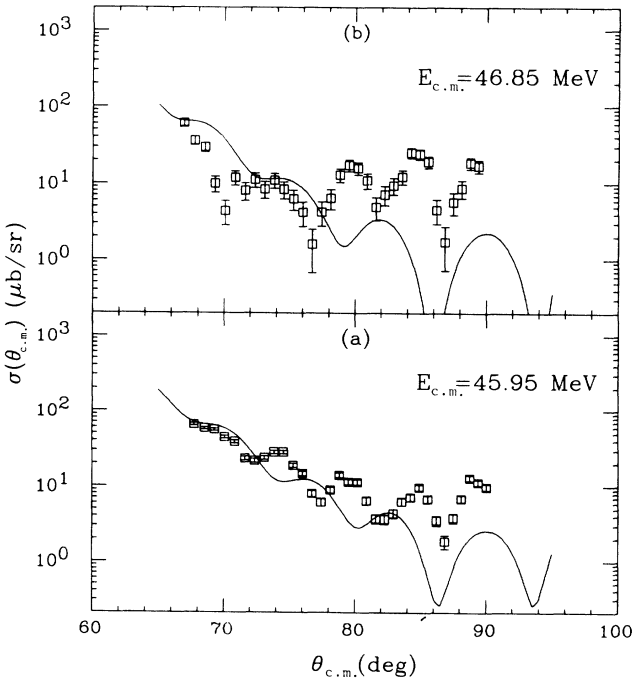

FIG. 7. Off-resonance elastic-scattering angular-distribution data for (a) $E_{\text{c.m.}}=45.95$ MeV and (b) $E_{\text{c.m.}}=46.85$ MeV. The curves correspond to optical-model calculations described in the text.

TABLE I. Optical-model parameters for $^{24}Mg+^{24}Mg$ elastic scattering from Betts (Ref. 32).

V_0 (MeV)	r_0 (fm)	a (fm)	W (MeV)	r_0' (fm)	a' (fm)	r_{0C} (fm)
38.00	1.195	0.642	25.20	1.166	0.659	1.20

If, instead, we view the data in the coordinate system with the quantization axis taken along the normal to the scattering plane, we find little difference between the energy dependences of the two substate cross sections. In this coordinate system, the Bohr theorem demands that only the $|m|=0$ and 2 substates be populated.[34] Excitation-function data for the $|m|=0$ and 2 substates for the beam-axis coordinate system, as well as the calculated alignment parameter P_{ZZ}, appear in Fig. 9. The alignment is defined by[33]

$$P_{ZZ}=\frac{1}{J(2J-1)}\left[\sum_m 3m^2P_m-J(J+1)\right]. \quad (5)$$

We find both resonance and background rather strongly aligned, with an average P_{ZZ} around 0.5. In contrast, for resonances in the $^{12}C+^{12}C$ system, strong enhancements in the alignment accompanied peaks in the inelastic-scattering cross section.[22]

We now consider the particle angular distributions for individual magnetic substates in the beam-axis coordinate system. Angular-distribution data obtained at $E_{c.m.}=45.70$ MeV, at the peak of one resonance, appear in Fig. 10. Figure 11 contains similar data for the resonance at $E_{c.m.}=46.65$ MeV, where we have summed the data for the six excitation-function points around the peak in order to obtain sufficient statistics to perform γ-ray angular distribution fits. For both sets of data, in the total cross section, as well as the $m=0$ angular distribution, we see prominent oscillations, very nearly in phase with a squared Legendre polynomial of order 34. The data for $|m|=1$ and 2 behave very differently, with little or no oscillatory structure. Also, both the $|m|=1$ and 2 angular distributions increase notably toward forward angles, presumably reflecting the contribution of direct potential scattering.

Off-resonance magnetic-substate angular-distribution data obtained at $E_{c.m.}=45.95$ MeV appear in Fig. 12. The differences between the on- and off-resonance data are clear and striking. In the $m=0$ data, the magnitude and oscillatory behavior of the back-angle cross section are substantially reduced, compared to their on-resonance couterparts. The back-angle cross sections for the $|m|=1$ and 2 substates are also considerably smaller, although the rise at forward angles due to potential scattering persists. The stark contrast between the $m=0$

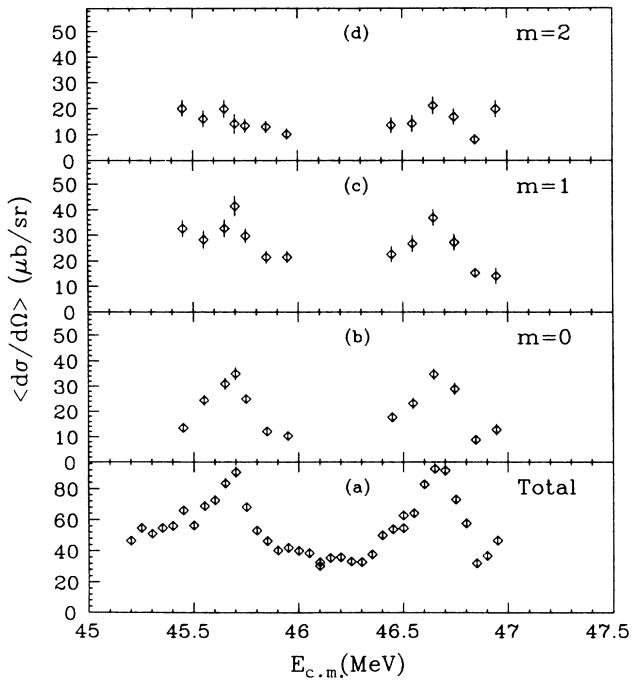

FIG. 8. Magnetic-substate excitation-function data for $^{24}Mg+^{24}Mg$ single 2^+ inelastic scattering, averaged over $66°\leq\theta_{c.m.}\leq 93°$. (a) Total cross section. (b), (c), and (d) Cross sections for $|m|=0$, 1, and 2, respectively. Quantization axis is along the beam.

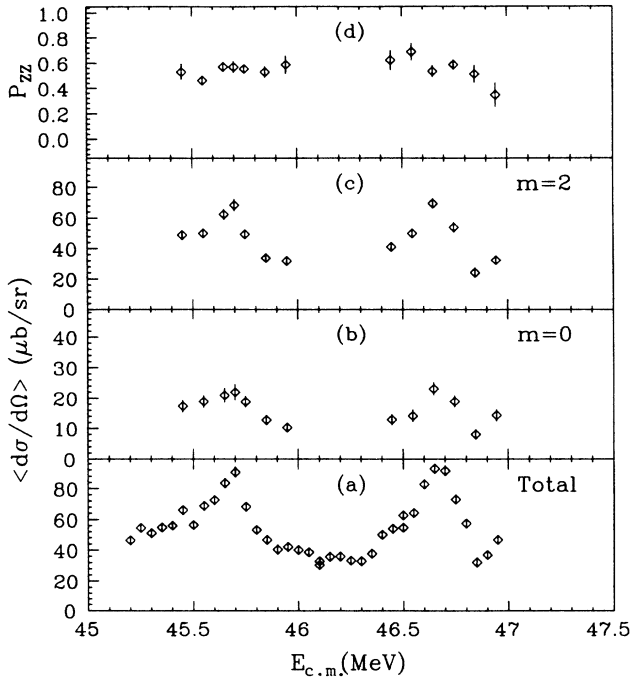

FIG. 9. Magnetic-substate excitation-function data for $^{24}Mg+^{24}Mg$ single 2^+ inelastic scattering, averaged over $66°\leq\theta_{c.m.}\leq 95°$. (a) Total cross section. (b) and (c) Cross sections for $|m|=0$ and 2, respectively. (d) Alignment P_{ZZ}. Quantization axis is along the normal to the scattering plane.

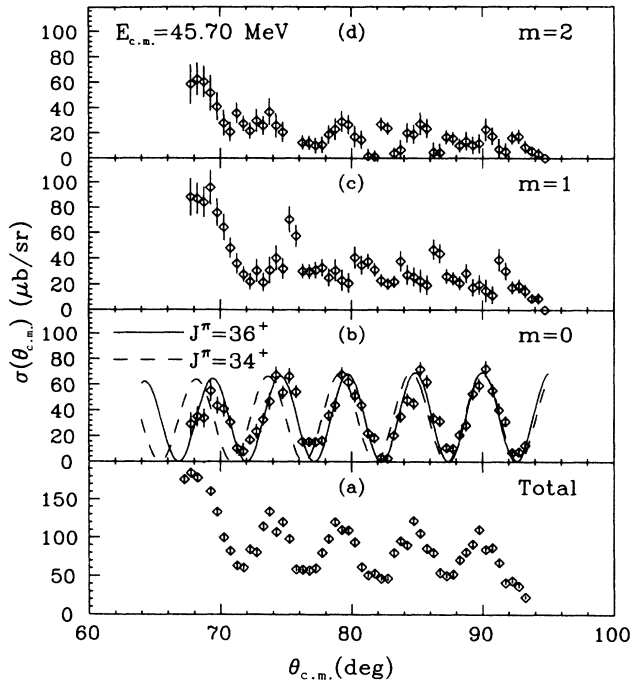

FIG. 10. Magnetic-substate angular-distribution data for ^{24}Mg+^{24}Mg single 2^+ inelastic scattering for $E_{c.m.}=45.70$ MeV. (a) Total cross section. (b), (c), and (d) Cross section for $|m|=0$, 1, and 2, respectively. The fits to the $m=0$ angular distribution are described in the text, and correspond to $J^{\pi}=34^+$ (dashed curve) and 36^+ (solid curve), with a dominant decay l value of $l=J-2$ in each case.

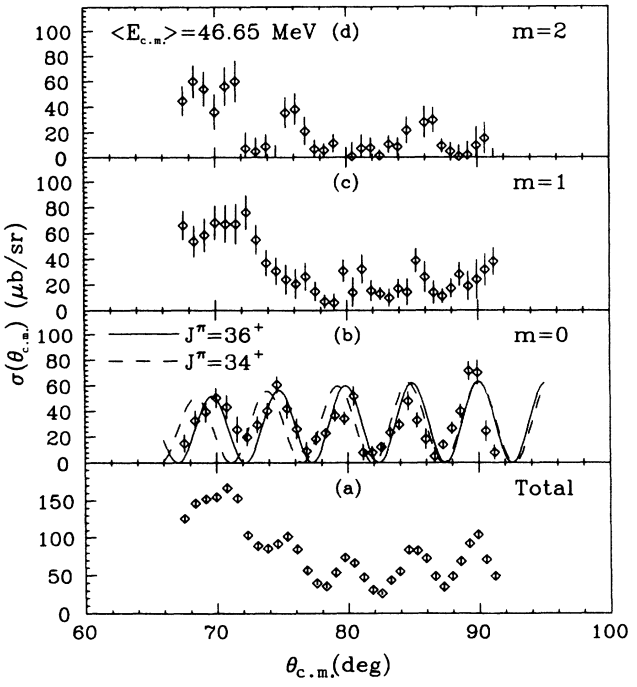

FIG. 11. Magnetic-substate angular-distribution data for ^{24}Mg+^{24}Mg single 2^+ inelastic scattering, summed from $46.45 \le E_{c.m.} \le 46.95$ MeV. (a) Total cross section. (b), (c), and (d) Cross section for $|m|=0$, 1, and 2, respectively. The fits to the $m=0$ angular distribution are described in the text and correspond to $J^{\pi}=34^+$ (dashed curve) and 36^+ (solid curve), with a dominant decay l value of $l=J-2$ in each case.

angular distribution data in Figs. 10 and 11, and those in Fig. 12 clearly demonstrates that the structure observed in the on-resonance data reflects a clean signature for the resonance spin and decay l value.

We can draw several conclusions from these data. The very small amount of background seen in the $m=0$ excitation-function data suggest that spectroscopic information obtained from the $m=0$ angular distribution will be relatively free of background contamination. Also, the strongly oscillatory character of the $m=0$ angular distribution for the two resonances indicates that a single l value, $l=34$, dominates the resonance decay in this channel for the states at $E_{c.m.}=45.70$ and 46.65 MeV. For the $E_{c.m.}=46.65$ MeV resonance data, the process of summing over energy will increase the background contribution somewhat. The off-resonance angular-distribution data obtained at $E_{c.m.}=45.95$ MeV suggest, however, that this contamination is quite small.

In order to quantitatively interpret our magnetic-substate excitation-function and angular-distribution data, we consider the transition amplitude for single 2^+ inelastic scattering. In this case, the transition amplitude for a given magnetic substate m is given by[35]

$$A_m(\mathbf{k}_b)=\frac{2\pi}{ik}\sum_{l_i,l_f}\left[\frac{(2l_i+1)}{4\pi}\right](l_f 2-mm|l_i 0)\times e^{i(\sigma l_i+\sigma l_f)}\eta_{l_f}^{l_i}Y_{l_f}^{-m}(\mathbf{k}_b)^{*}\,, \quad (6)$$

where l_i and l_f are the partial waves in the entrance and

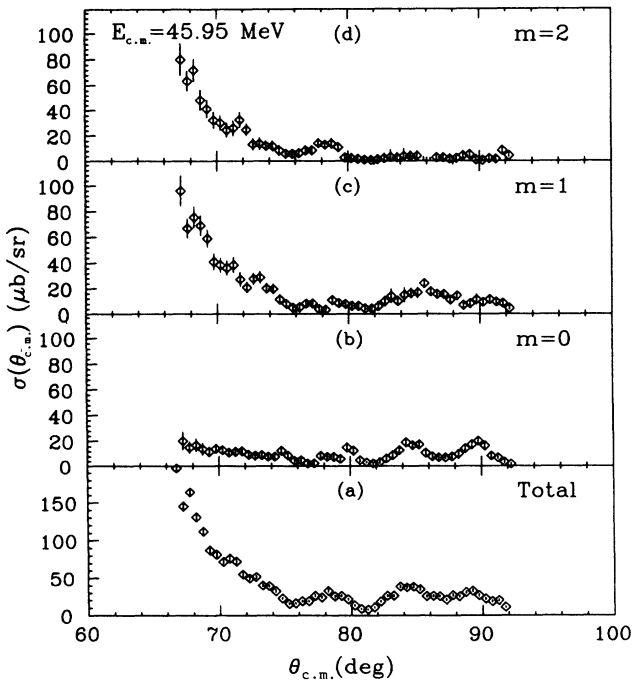

FIG. 12. Magnetic-substate angular-distribution data for ^{24}Mg+^{24}Mg single 2^+ inelastic scattering for $E_{c.m.}=45.95$ MeV. (a) Total cross section. (b), (c), and (d) Cross section for $|m|=0$, 1, and 2, respectively.

exit channels, σ_{l_i} and σ_{l_f} are phase shifts for each partial wave, and the η are scattering matrix elements. The inelastic-scattering cross section for a given magnetic substate m is then given simply as

$$\sigma_m(\theta_{\text{c.m.}}) = |A_m(\mathbf{k}_b)|^2 . \quad (7)$$

In the case of the decay of an isolated resonance with spin J, we restrict the sum in Eq. (6) to only the terms with $l_i = J$ and $l_f = J, J\pm 2$. For a single decay l value, the resonance magnetic-substate angular distributions will be given by $\sigma_m(\theta_{\text{c.m.}}) \sim |Y_l^{-m}(\theta_{\text{c.m.}})|^2$. Furthermore, the ratios of the angle-averaged magnetic-substate cross sections will be roughly in proportion to the squares of the Clebsch-Gordan coefficients $|(l2-mm|J0)|^2$, with an additional factor of 2 for nonzero magnetic substates.

Table II summarizes the results for resonance and background contributions to the magnetic-substate cross sections, for the two resonances we studied. Also listed in Table II are the asymptotic values of the Clebsch-Gordan coefficients $|(l2-mm|J0)|^2$, valid for $J, l \gg 1$, for the aligned (or antialigned) configuration ($l = J\pm 2$), and the nonaligned configuration ($l = J$). If we assume that a single l value dominates the decay, we find that the measured cross-section ratios are consistent only with $l = J\pm 2$ as the dominant decay l value. It is also simple to show that for a single decay l value, the magnetic-substate populations in the normal coordinate system are given by[36] $P_m \sim \delta_{|J-l|,m}$. The values of $\sigma_{|m|}$ in this coordinate system, as well as the measured values of the alignment P_{ZZ}, are similarly consistent with $l = J\pm 2$, rather than $J = l$, dominating the resonance decay. In order to generate a fit to the $m = 0$ angular-distribution data, we parametrize the magnetic-substate cross section as

$$\sigma_m(\theta_{\text{c.m.}}) = \left| \sum_l A_l (l2-mm|J0) Y_l^{-m}(\theta_{\text{c.m.}}) \right|^2 . \quad (8)$$

We choose values for the three complex amplitudes A_l to reproduce the measured angle-averaged resonance substate cross sections. Table III lists the values of the A_l obtained at $E_{\text{c.m.}} = 45.70$ and 46.65 MeV. The resulting fits to the $m = 0$ angular-distribution data in Figs. 10 and 11 are calculated for $J = 34$ (dashed line) and $J = 36$ (solid line), using the amplitudes given in Table III. For both sets of data, $J = 36$ yields the superior fit, and we assign

TABLE III. Resonance decay l value amplitudes for single 2^+ inelastic scattering.

l	$E_{\text{RES}} = 45.70$ $\lvert A_l \rvert$	$E_{\text{RES}} = 46.65$ MeV $\lvert A_l \rvert$
$J-2$	0.97	0.93
J	0.24	0.31
$J+2$	0.06	0.18

$J^\pi = 36^+$ for the resonances seen at $E_{\text{c.m.}} = 45.70$ and 46.65 MeV. Angular momentum coupling strongly favors the dominance of the lowest allowed l value, and while the cross-section data can be reproduced assuming a predominantly antialigned configuration, no physical argument supports this choice.

D. 2^+-2^+ excitation

We used similar particle-γ correlation methods to study the mutual 2^+ excitation in ^{24}Mg+^{24}Mg inelastic scattering. We subjected these data to two separate analyses. First we analyzed the data by considering the direction of only one of the two γ rays from the inelastic scattering. From these results we obtained magnetic-substate excitation functions and angular distributions as for the single 2^+ inelastic scattering channel. We then performed an analysis that involved the directions of both γ rays arising from the inelastic scattering. As described in Sec. III, these results provide us with correlated magnetic-substate population parameters which describe the correlated orientation of the spins of both ^{24}Mg nuclei.[22,27] The counting statistics for this second analysis were somewhat limited, and for this procedure we were able to obtain only particle-angle-averaged excitation-function results.

Figure 13 contains magnetic-substate excitation-function data for mutual 2^+ inelastic scattering, where the quantization axis is chosen to lie along the beam. As described above, the results are averaged over the direction of one γ ray. The results are strikingly similar to those for the single 2^+ case. The $m = 0$ substate again shows the strongest resonance behavior, with a peak-to-background ratio of approximately 3 to 1. The alignment with respect to the normal to the scattering plane also appears in Fig. 13. As was the case with the single 2^+ excitation, P_{ZZ} exhibits relatively little structure. The only

TABLE II. Resonance and background values of $\sigma_{|m|}$ in (μb/sr).

Beam axis	$E_{\text{RES}} = 45.70$ MeV Background	Resonance	$E_{\text{RES}} = 46.65$ MeV Background	Resonance	$l = J\pm 2$ $(2-\delta_{m,0}) \times \lvert(l2-mm\lvert J0)\rvert^2$	$l = J$
σ_0	10	25	10	28	$\frac{3}{8}$	$\frac{1}{4}$
σ_1	26	16	15	18	$\frac{1}{2}$	0
σ_2	15	~0	10	~0	$\frac{1}{8}$	$\frac{3}{4}$
Normal axis					$\delta_{\lvert J-l\rvert m}$	
σ_0	11	8	14	7	0	1
σ_2	40	29	33	37	1	0
P_{ZZ}	0.52±0.06	0.51±0.08				

notable features in P_{ZZ} for the mutual 2^+ channel are very moderate dips at the two resonance peak energies.

The corresponding magnetic-substate angular-distribution data for mutual 2^+ inelastic scattering appear in Figs. 14–16. Again, for the resonance at $E_{\text{c.m.}}=46.65$ MeV, we summed the data from six energies over the peak to obtain adequate γ-ray statistics. As was the case with the single inelastic channel, on resonance the $m=0$ angular distributions contain prominent oscillations. The $|m|=1$ and 2 substate distributions are smoother and contain the familiar monotonic rise at forward angles. Interestingly, the oscillations in the on-resonance $m=0$ angular distributions are again nearly in phase with a Legendre polynomial squared of order 34, implying that both resonances decay predominantly through $l=34$ in mutual, as well as single, 2^+ inelastic scattering.

To put this conjecture on a more quantitative footing, we consider the transition amplitude for mutual inelastic scattering. For a given value of J, the transition amplitude for a combination of magnetic substates (m_1,m_2) now contains a sum over an intermediate spin S, as well as five possible decay l values $l=J, J\pm2$, and $J\pm4$, and is given by[35]

$$A_{m_1,m_2}(\mathbf{k}_b)=\frac{2\pi}{ik}\sum_{l_f,S}(22m_1m_2|Sm_S)(l_fS-m_Sm_S|J0)e^{i(\sigma_{l_f}+\sigma_J)}\eta^J_{l_fS}\left[\frac{(2J+1)}{4\pi}\right]^{1/2}Y_{l_f}^{-m_S}(\mathbf{k}_b)^* \ . \tag{9}$$

In order to generate fits to the $m=0$ data in Figs. 14 and 15, we assume a resonance of spin $J^\pi=36^+$, decaying through only a single l value. Also, since the oscillatory structure of the calculated angular distribution in Eq. (9) is relatively insensitive to the choice of $\eta_{l_fS_J}$, we further simplify the situation by fixing $|\eta^J_{l_fS}|=1$ for all values of S. Finally, we must sum over one magnetic-substate quantum number:

$$\sigma_0(\theta_{\text{c.m.}})=\sum_{m_1}\sigma_{m_1,m_2},\quad m_2=0 \ . \tag{10}$$

The curves in Figs. 14 and 15 correspond to calculations with $l=32$ (dashed curve) and $l=34$ (solid curve). Despite the rather simple assumptions used to generate these curves, the $l=34$ fit reproduces both $m=0$ angular distributions surprisingly well. The curve calculated assuming that the lowest allowed l value, $l=32$, dominates the decay, agrees rather poorly with the data.

We now consider the case where we measure the angles of both γ rays from mutual 2^+ inelastic scattering. Here we choose the quantization axis to lie along the normal to the scattering plane. Figure 17 shows angle-averaged

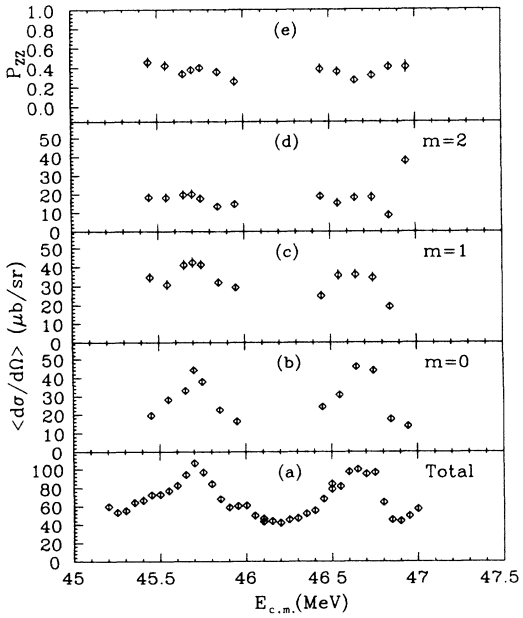

FIG. 13. Magnetic-substate excitation-function data for ^{24}Mg+^{24}Mg mutual 2^+ inelastic scattering, averaged over $66°\le\theta_{\text{c.m.}}\le93°$. The data are also averaged over the direction of one of the two γ rays. (a) Total cross section. (b), (c), and (d) Cross sections for $|m|=0$, 1, and 2, respectively. Quantization axis for (b), (c), and (d) is along the beam. (e) Alignment P_{ZZ}, with respect to the normal to the scattering plane.

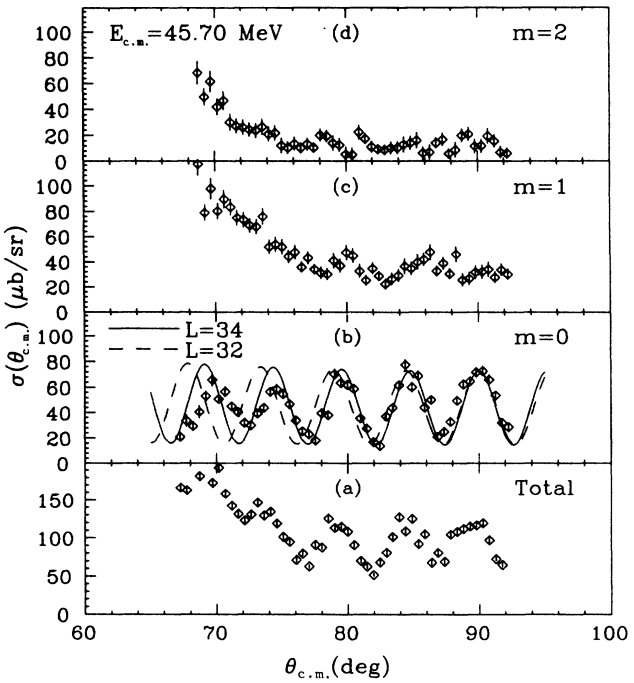

FIG. 14. Magnetic-substate angular-distribution data for ^{24}Mg+^{24}Mg mutual 2^+ inelastic scattering for $E_{\text{c.m.}}=45.70$ MeV. (a) Total cross section. (b), (c), and (d) Cross section for $|m|=0$, 1, and 2, respectively. The data are averaged over the direction of one of the two γ rays. The fits to the $m=0$ angular distribution are described in the text and correspond to $J^\pi=36^+$, $l=32$ (dashed curve) and $l=34$ (solid curve). Quantization axis is along the beam.

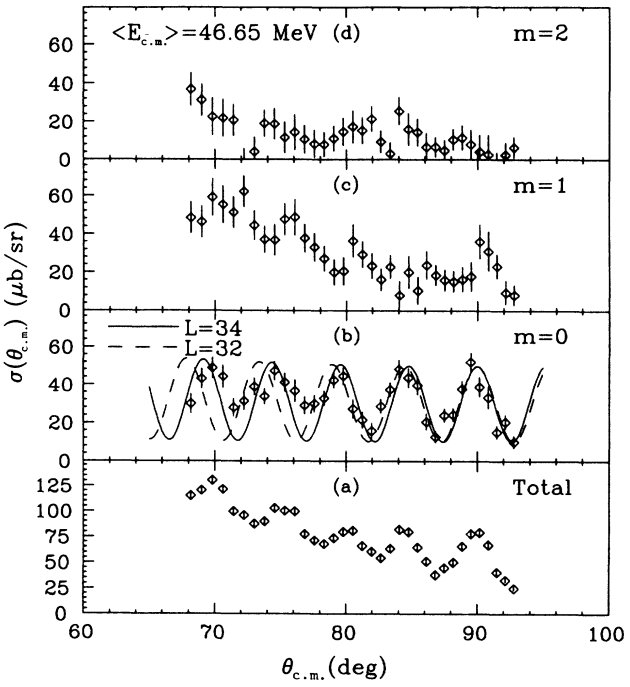

FIG. 15. Magnetic-substate angular-distribution data for ^{24}Mg+^{24}Mg mutual 2^+ inelastic scattering, summed from $46.45 \leq E_{c.m.} \leq 46.95$ MeV. (a) Total cross section. (b), (c), and (d) Cross section for $|m|=0$, 1, and 2, respectively. The data are averaged over the direction of one of the two γ rays. The fits to the $m=0$ angular distribution are described in the text and correspond to $J^{\pi}=36^+$, $l=32$ (dashed curve) and $l=34$ (solid curve). Quantization axis is along the beam.

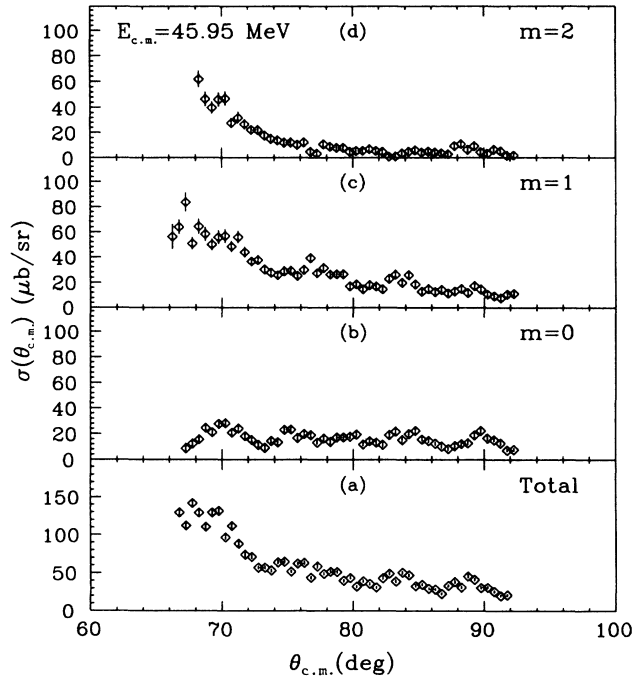

FIG. 16. Magnetic-substate angular-distribution data for ^{24}Mg+^{24}Mg mutual 2^+ inelastic scattering for $E_{c.m.}=45.95$ MeV. (a) Total cross section. (b), (c), and (d) Cross section for $|m|=0$, 1, and 2, respectively. The data are averaged over the direction of one of the two γ rays. Quantization axis is along the beam.

correlated magnetic-substate excitation-function data over the two resonances studied. In this case, the Bohr theorem demands that only even values of $|m_1|+|m_2|$ may contribute to the cross section.[22,26] In our fits, we found that the combination $(m_1,m_2)=(0,0)$ made a negligible contribution to the cross section, and that σ_{00} was consistent with zero at each energy.

As with the alignment data for the single 2^+ excitation, the results for the correlated substate cross sections are rather different from those seen in ^{12}C+^{12}C inelastic scattering.[22] In the ^{12}C+^{12}C case, the mutually aligned configuration with $(|m_1|,|m_2|)=(2,2)$ dominated the resonance cross section. Here, while the (2,2) component is fairly strong, little structure appears in the excitation function over either resonance. Instead, the partially aligned component σ_{20} shows the clearest resonance peak.

We can compare the correlated alignment results with the expectations for the correlated substate populations one obtains from the observed decay l values. For a resonance with spin 36, one expects a mutually aligned configuration with $(|m_1|,|m_2|)=(2,2)$ when the lowest l value dominates the decay. For a decay l value of 34, the partially aligned configuration with $|m_1|+|m_2|=2$ would show the strongest resonance behavior. We recall that for both resonances, the observed decay l value was indeed 34, with a partially aligned configuration containing the most resonance strength. These two measurements thus provide us with a clear confirmation of our expectations for the interplay between angular momen-

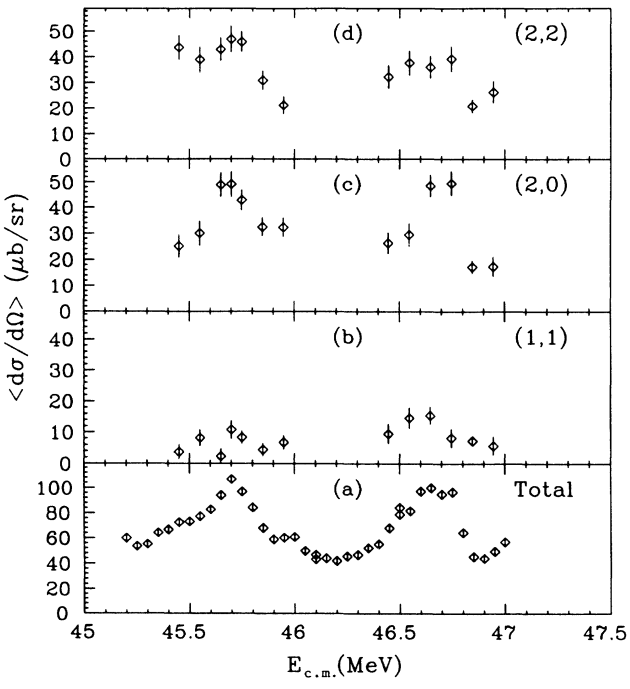

FIG. 17. Correlated magnetic-substate excitation-function data for ^{24}Mg+^{24}Mg mutual inelastic scattering averaged over $66° \leq \theta_{c.m.} \leq 93°$. (a) Total cross section. (b), (c), and (d) $(|m_1|,|m_2|)=(1,1)$, (2,0), and (2,2), respectively. Quantization axis is along the normal to the scattering plane.

tum coupling and spin alignment.

E. Higher excitations and transfer channels

We have also obtained spin-alignment data for excitations involving higher-lying members of the ground-state rotational band in $^{24}Mg+^{24}Mg$ inelastic-scattering. Figure 18 shows the alignment, as well as the inelastic-scattering cross sections as a function of center-of-mass energy for several strongly excited channels in $^{24}Mg+^{24}Mg$. The cross-section data are those of Zurmühle *et al.* from Ref. 6. As with the single and mutual 2^+ inelastic channels, the alignment for these higher excitations depends very little upon energy. The energy-averaged alignment as a function of Q value for the two resonances we studied appears in Fig. 19. For Q values of $|Q| \geq 4$ MeV, the alignment peaks at the mutual 4^+ excitation at $Q = -8.24$ MeV. The large values for both the cross section and the alignment for this excitation may suggest that this channel lies close to the classical sticking configuration, which in our case favors a roughly equal sharing of ~ 9 units of angular momentum.

Alignment data for higher excited states in $^{24}Mg+^{24}Mg$ inelastic scattering at an energy of $E_{c.m.} = 45.7$ MeV have also been reported by the Munich group[37] using the out-of-plane method.[22] For comparison, these data also appear in Fig. 19(a). The general trends in the two sets of data are somewhat similar. In both data sets, the alignment increases toward more negative Q values. In the Munich results, however, P_{ZZ} remains quite large, ~ 0.8, for Q values of $Q < -5.0$ MeV, whereas for the present data, the alignment peaks at $Q = -8.24$ MeV, and then decreases.

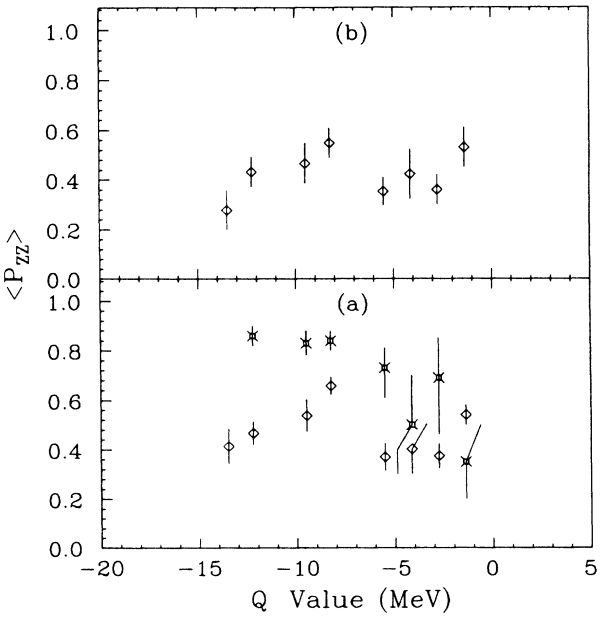

FIG. 19. Energy-averaged spin-alignment data for $^{24}Mg+^{24}Mg$ inelastic scattering. (a) $45.45 \leq E_{c.m.} \leq 45.95$ MeV, (b) $46.45 \leq E_{c.m.} \leq 46.95$ MeV. The open symbols are the present data. The crosses in (a) are the data of Mattis *et al.* (Ref. 37).

Similar data for the 1-α-particle transfer channel leading to $^{20}Ne+^{28}Si$ appear in Fig. 20. Here the dependence on Q value is much smoother that in the $^{24}Mg+^{24}Mg$ case, and the overall magnitude of the alignment is reduced. It is possible that the weak branching strength for these resonances in the $^{20}Ne+^{28}Si$ channel, as well as the

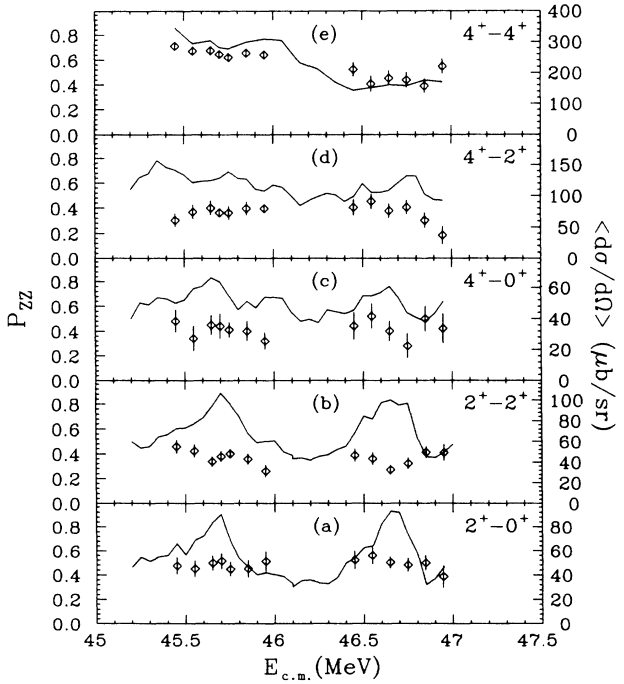

FIG. 18. Spin-alignment (points) and cross-section (solid line) excitation-function data for several strongly excited channels in $^{24}Mg+^{24}Mg$ inelastic scattering.

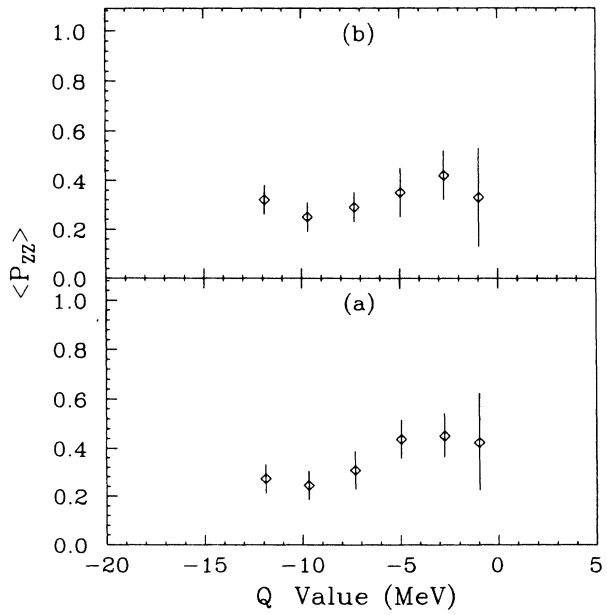

FIG. 20. Energy-averaged spin-alignment data for the α-transfer reaction $^{24}Mg(^{24}Mg,^{20}Ne)^{28}Si$. (a) $45.45 \leq E_{c.m.} \leq 45.95$ MeV, (b) $46.45 \leq E_{c.m.} \leq 46.95$ MeV.

smaller values of the alignment, result from the preference for symmetric fission of states with very high angular momentum in ^{48}Cr.

V. SUMMARY AND MODEL CALCULATIONS

A. Summary

The present results, coupled with systematic trends in elastic- and inelastic-scattering angular distributions, allow us to suggest tentative spin assignments for the resonances observed at higher energies. Elastic-scattering angular distributions from Zurmühle *et al.*[12] appear in Fig. 21 for several resonances. We have already assigned spin 36^+ for the two resonances at $E_{c.m.}=45.70$ and 46.65 MeV. For the remaining two peaks in the range $45 \le E_{c.m.} \le 47$ MeV, the similarity of the resonance elastic- and inelastic-scattering angular distributions to those for resonances with known spin also suggest tentative spin assignments of $J^\pi=36^+$. For the peaks near $E_{c.m.}=50.5$ and 54.0 MeV, the resonance angular distributions, while not sufficient by themselves to make spin assignments, indicate that the dominant angular momenta increase by two units for each group. These arguments yield tentative spin assignments of $J^\pi=38^+$ and 40^+ for the resonances near $E_{c.m.}=50.5$ and 54.0 MeV, respectively, as shown in Fig. 22. Here we emphasize that these assignments are tentative and require more detailed measurements of the type described above to provide a rigorous identification of the spins involved.

It is interesting to compare the suggested resonance spins to the values of the grazing angular momentum obtained from optical-model calculations for the ^{24}Mg+^{24}Mg system in the present energy range. In particular, the spin of the resonance at $E_{c.m.}=45.70$ MeV is approximately 4 units higher than the elastic-scattering grazing angular momentum l_{gr}, which is near 32 at this energy. This result suggests that in the resonance configuration, the ^{24}Mg+^{24}Mg system can sustain more angular momentum than it could in a random orientation. A resonance configuration which would explain this phenomenon is one in which the two prolate-deformed ^{24}Mg nuclei interact pole-to-pole, with their symmetry axes on line. With the large quadrupole deformation of ^{24}Mg, such a complex would have a considerably larger average moment of inertia than a randomly oriented configuration. The effective grazing angular momentum at a given energy for such a complex would be larger than that calculated naively, allowing the population of higher spin resonances. We will also find that we are led to consider this same model for the ^{24}Mg+^{24}Mg resonance configuration from a theoretical point of view.

B. Model calculations

In an attempt to relate the observed resonance behavior to the structure of the composite system ^{48}Cr at high spin and excitation energy, we employed the rotating

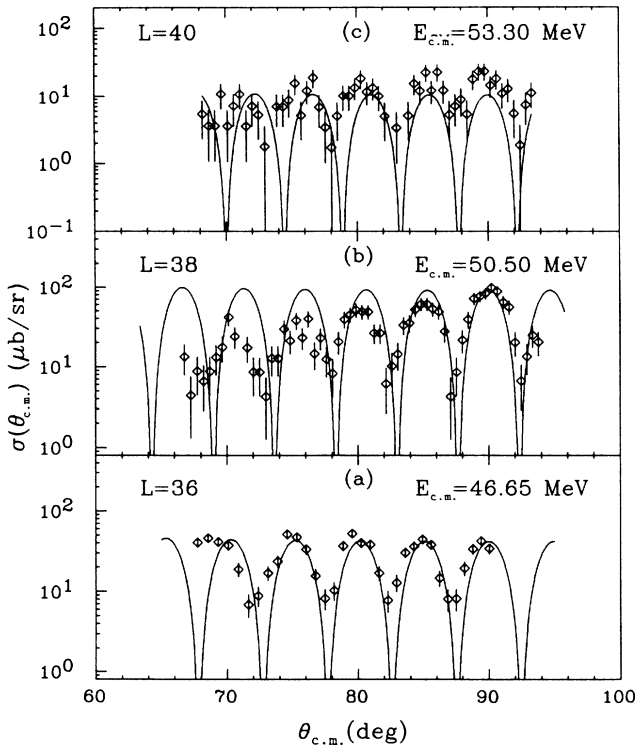

FIG. 21. Resonance elastic-scattering angular-distribution data from Zurmühle (Ref. 9), for (a) $E_{c.m.}=50.5$ MeV, (b) $E_{c.m.}=54.0$ MeV. The curves correspond to squared Legendre polynomials of order (a) 36, (b) 38, and (c) 40.

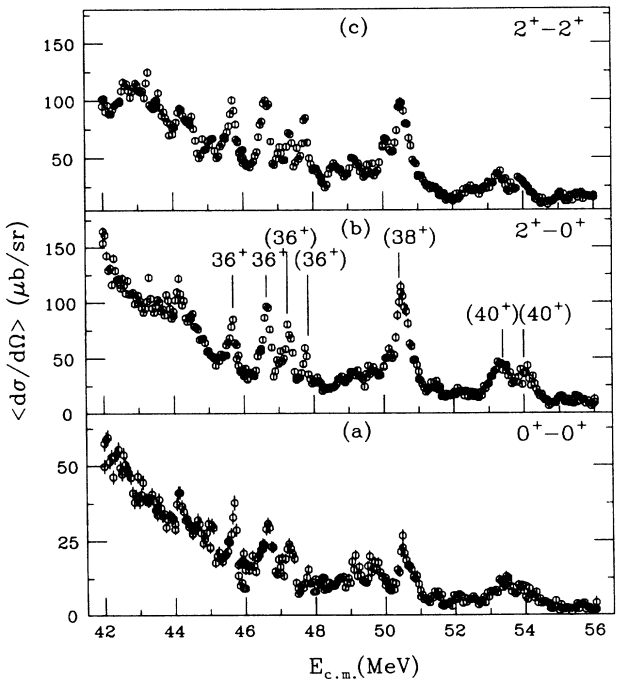

FIG. 22. Excitation-function data from Zurmühle *et al.* (Refs. 6 and 9) for (a) elastic scattering, (b) single 2^+ inelastic scattering, and (c) mutual 2^+ inelastic scattering, averaged over $66° \le \theta_{c.m.} \le 93°$. The spin assignments are discussed in the text.

liquid drop model (RLDM). Although this model is a purely macroscopic one which ignores the quantum nature of the nuclear system and changes in the potential energy due to shell corrections, it can still be quite useful in identifying trends in the study of highly deformed, rotating nuclei. Liquid drop model calculations for the $^{26}Mg+^{26}Mg \rightarrow ^{52}Cr$ system performed by Broglia *et al.*[38] suggested stable, highly deformed configurations at very high spin in the composite system, near $l=40-50$. In the present calculations we examine similar structures in ^{48}Cr.

Our calculations were carried out using both a sharp-surface approximation and a diffuse-surface folding Yukawa formulation of the RLDM. The liquid drop parameters were those taken from Cohen, Plasil and Swiatecki.[39] For our calculations we included quadrupole, hexadecapole, and triaxial deformations. It was found that at very high spins the equilibrium shapes obtained from these calculations tended strongly toward axial symmetry. Figure 23 shows a contour plot of a RLDM potential-energy surface calculated for spin 32. Here, the triaxial deformation parameter γ is fixed at its equilibrium value of 4°. A well-defined potential minimum appears at $(\beta_2,\beta_4)=(0.8,0.2)$. The dashed line marks the path from the potential minimum to the fission barrier, which, at this spin, has a height of approximately 4 MeV above the energy minimum. Also shown in Fig. 23 are the shapes corresponding to the points labeled along the fission path. The shape at the fission barrier top (point "3") is strongly reminiscent of the pole-to-pole grazing collision between two ^{24}Mg nuclei suggested by the relatively high values of the spins of the observed resonances.

Potential-energy curves relative to the potential-energy minimum appear in Fig. 24, for several values of l. Here the potential energy $V_{LD}(\beta_2)$ is plotted along the fission path. Both the equilibrium deformation and the height of the fission barrier change quite rapidly with increasing spin. This result suggests that lifetimes of states in such a system would decrease as a function of increasing spin. Such a trend is precisely what we observe in the excitation curves in Figs. 1 and 22. The resonances near 45 MeV are quite narrow, with widths on the order of 150 keV, while the states near 54 MeV are much wider ($\Gamma \sim 800$ keV). In addition, the calculated differences between potential-energy minima for successive angular momenta in the $l \sim 36$ region are approximately 3.5 MeV, a value very near the observed spacing between adjacent groups of resonances.

Recently some more realistic calculations using the two center shell model (TCSM) have been performed by Maass and Scheid.[40] The potential energy in these calculations is chosen to vanish at infinite separation. The calculated minimum energy of 42 MeV is in quite good agreement with measured resonance energies of $E_{c.m.} \sim 45$ MeV for $J^{\pi}=36^{+}$. The highly deformed equilibrium shape obtained from these calculations also closely resembles a pole-to-pole configuration of two ^{24}Mg nuclei. These calculations strongly support the notion that the resonances observed in $^{24}Mg+^{24}Mg$ scattering correspond to the formation and subsequent fission of highly deformed, high spin states in the composite system ^{48}Cr.

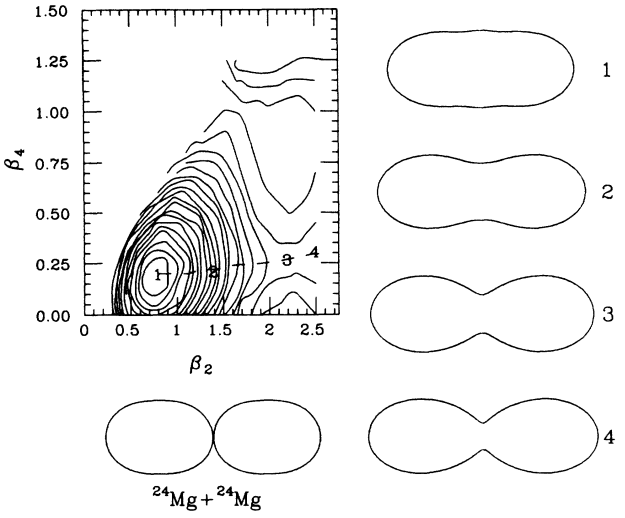

FIG. 23. RLDM potential-energy surface for ^{48}Cr at $l=32$. The contour lines are 200 keV apart. The shapes labeled 1, 2, 3, and 4 correspond to the RLD shape at the points indicated on the potential-energy surface. Also plotted is a pole-to-pole grazing collision between two ^{24}Mg nuclei.

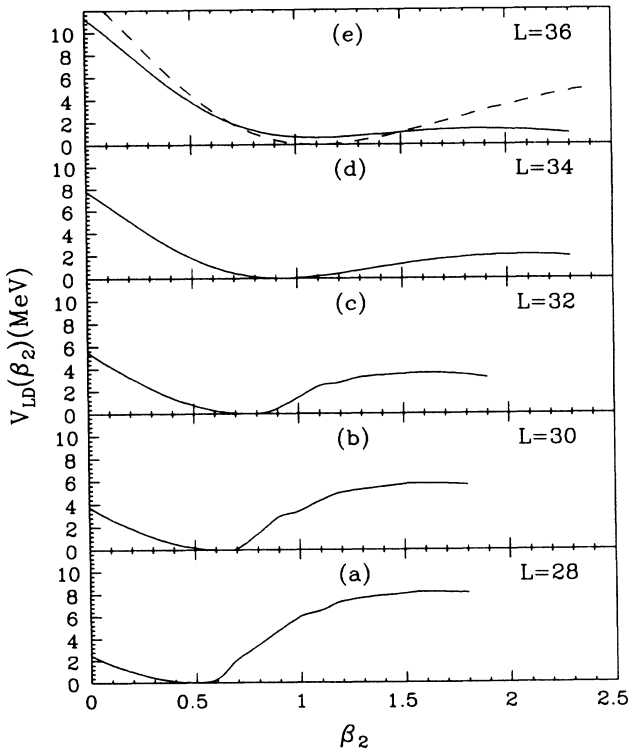

FIG. 24. RLDM fission barrier shapes for several angular momenta. The dashed curve in (e) corresponds to the fission barrier obtained from a calculation using a sharp cutoff approximation for the nuclear surface.

VI. CONCLUSIONS

The present results clearly demonstrate that particle-γ angular correlation techniques can serve as a powerful tool for examining resonance behavior in heavy-ion scattering. The spectroscopic information obtained from these measurements is much less sensitive to interference from nonresonant processes and allows unambiguous identification of the angular momenta contributing to the resonance. In particular, these data suggest spin assignments of $J^{\pi}=36^{+}$ for the resonances at $E_{\text{c.m.}}=45.70$ and 46.65 MeV in $^{24}\text{Mg}+^{24}\text{Mg}$ elastic and inelastic scattering. We also find that for the mutual 2^{+} excitation, our correlated alignment results agree well with what one expects for the given combination of resonance spin and decay l values. The observed resonance spins are about 4 units of angular momentum higher than the calculated elastic channel grazing partial wave. This discrepancy leads us to consider a specific configuration, that of a pole-to-pole grazing collision between the two heavy ions. This picture of the resonance process is supported by model calculations which lead to highly deformed equilibrium shapes in ^{48}Cr at spins near $30-40\hbar$, and saddle-point shapes that closely resemble a grazing collision between two deformed ^{24}Mg nuclei.

While the present results grant us considerable new insight into the phenomenon of resonance behavior in the $^{24}\text{Mg}+^{24}\text{Mg}$ system, several important questions remain unanswered. It is not yet clear why for each spin the resonance strength is split between several distinct peaks. This splitting could possibly reflect the importance of coupling to vibrational degrees of freedom.[41] Also, the total resonance cross section, obtained from summing the strength from all observed decay channels, is only a fraction of the total resonance cross section given by $\sigma_R=4\pi(2J+1)\lambda\!\!\!^{-2}$. Possibly, some of this strength is lost to the population of particle-unbound final states in ^{24}Mg.

In addition, at this point more sophisticated calculations of the structure of ^{48}Cr at high spin would prove quite useful. In particular, calculations within the framework of the cranked Nilsson-Strutinsky formalism could provide us with more realistic fission barrier shapes, as well as a better estimate of the location of the yrast levels in ^{48}Cr. Also, the modification of the potential-energy surface in going from α-particle systems to those with an additional neutron could help to explain resonance systematics. Some preliminary calculations are available.[11] To provide a better theoretical picture of resonances in these systems, however, a comprehensive survey of cranked-shell-model results for very high spin in the $A\sim 50$ mass region is necessary. Finally, our results suggest that certain other heavy-ion systems should show prominent resonance behavior of the kind seen in $^{24}\text{Mg}+^{24}\text{Mg}$. Should the deformation of the participating nuclei in the entrance and exit channels play an important role, systems involving the strongly deformed ^{20}Ne nucleus, such as $^{20}\text{Ne}+^{24}\text{Mg}$ and $^{20}\text{Ne}+^{20}\text{Ne}$, would be quite promising areas of study.

ACKNOWLEDGMENTS

We wish to thank H. T. Fortune and D. P. Balamuth for many helpful discussions. This work was supported by the National Science Foundation. The Oak Ridge National Laboratory was operated by Martin Marietta Energy Systems, Inc., under Contract No. DE-AC05-84OR-21400, with the U.S. Department of Energy.

*Present address: Physics Division, Argonne National Laboratory, Argonne, IL 60439.

†Present address: Indiana University Cyclotron Facility, Bloomington, IN 47405.

‡Present address: Oak Ridge National Laboratory, Oak Ridge, TN 37830.

[1]D. A. Bromley, J. A. Kuehner, and E. V. Almqvist, Phys. Rev. **123**, 878 (1961).

[2]E. Almqvist, D. A. Bromley, J. A. Kuehner, and B. Whalen, Phys. Rev. **130**, 1140 (1963).

[3]M. L. Halbert, F. E. Durham, and A. van der Woude, Phys. Rev. **162**, 899 (1967).

[4]R. R. Betts, S. B. DiCenzo, and J. F. Peterson, Phys. Lett. **100B**, 117 (1981).

[5]R. R. Betts, B. B. Back, and B. G. Glagola, Phys. Rev. Lett. **47**, 23 (1981).

[6]R. W. Zurmühle, P. Kutt, R. R. Betts, S. Saini, F. Haas, and Ole Hansen, Phys. Lett. **129B**, 384 (1983).

[7]A. H. Wuosmaa, S. Saini, P. H. Kutt, S. F. Pate, R. W. Zurmühle, and R. R. Betts, Phys. Rev. C **36**, 1011 (1987).

[8]S. Saini, R. R. Betts, R. W. Zurmühle, P. H. Kutt, and B. K. Dichter, Phys. Lett. B **185**, 316 (1987).

[9]R. W. Zurmühle, J. Phys. Soc. Jpn. Suppl. **58**, 37 (1989).

[10]R. R. Betts, Nucl. Phys. **A447**, 257c (1986).

[11]R. R. Betts, in *Nuclear Physics with Heavy Ions*, edited by P. Braun-Munzinger (Harwood Academic, New York, 1984).

[12]P. H. Kutt, S. F. Pate, A. H. Wuosmaa, R. W. Zurmühle, Ole Hansen, R. R. Betts, and S. Saini, Phys. Lett. **155B**, 27 (1985).

[13]B. Bilwes, R. Bilwes, J. Diaz, J. L. Ferraro, D. Pocinac, and L. Stuttge, Nucl. Phys. **A463**, 731 (1987).

[14]B. Imanishi, Nucl. Phys. **A125**, 33 (1969).

[15]T. Matsuse, Y. Abe, and Y. Kondo, Prog. Theor. Phys. **59**, 1904 (1978).

[16]O. Tanimura and U. Mosel, Phys. Lett. **105B**, 334 (1981).

[17]R. L. Phillips, K. A. Erb, D. A. Bromley, and J. Weneser, Phys. Rev. Lett. **42**, 566 (1979).

[18]P. J. Twin, B. M. Nyako, A. H. Nelson, J. Simpson, M. A. Bentley, H. W. Cranmer-Gordon, P. D. Forsyth, D. Howe, A. R. Mokhtar, J. D. Morrison, J. F. Sharpey-Schafer, and G. Sletten, Phys. Rev. Lett. **57**, 811 (1986).

[19]A. J. Kirwin, G. C. Ball, P. J. Bishop, M. J. Godfrey, P. J. Nolan, D. J. Thornley, D. J. G. Love, and A. H. Nelson, Phys. Rev. Lett. **58**, 467 (1987).

[20]E. M. Beck, F. S. Stephens, J. C. Bacelar, M. A. Deleplanque, J. E. Draper, C. Duyar, and R. J. McDonald, Phys. Rev. Lett. **58**, 2182 (1987).

[21]B. Haas, P. Taras, S. Flibotte, F. Banville, J. Gascon, S. Cournoyer, S. Monaro, N. Nadon, D. Prevost, D. Thibault, J. K.

Johannson, D. M. Tucker, J. C. Waddington, H. R. Andrews, G. C. Bell, D. C. Radford, D. Ward, C. St. Pierre, and J. Dudek, Phys. Rev. Lett. **60**, 503 (1988).

[22]W. Trombik, W. Trautmann, F. Krug, W. Dünnweber, D. Konnerth, W. Hering, R. Singh, and D. Zeppenfeld, Phys. Lett. **135B**, 271 (1984).

[23]D. Konnerth, W. Dünnweber, W. Hering, W. Trautmann, W. Trombik, W. Zipper, D. Habs, W. Hennerici, H. J. Hennrich, R. Kroth, A. Lazzarini, R. Repnow, V. Metag, and R. S. Simon, Phys. Rev. Lett. **55**, 588 (1985).

[24]L. E. Cannell, R. W. Zurmühle, and D. P. Balamuth, Phys. Rev. Lett. **43**, 837 (1979).

[25]D. P. Balamuth, L. E. Cannell, and R. W. Zurmühle, Phys. Rev. C **23**, 2592 (1981).

[26]C. M. Jachinski, P. Braun-Munzinger, G. M. Berkowitz, R. H. Freifelder, M. Gai, R. L. McGrath, R. Paul, T. Renner, and C. D. Ulhorn, Phys. Lett. **87B**, 354 (1979).

[27]A. H. Wuosmaa, R. W. Zurmühle, P. H. Kutt, S. F. Pate, S. Saini, M. L. Halbert, and D. C. Hensley, Phys. Rev. Lett. **58**, 1312 (1987).

[28]M. Jääskeläinen, D. G. Sarantites, R. Woodward, F. A. Dilmanian, J. T. Hood, R. Jääskeläinen, D. C. Hensley, M. L. Halbert, and J. H. Barker, Nucl. Instrum. Methods **204**, 385 (1983).

[29]D. P. Balamuth, P. H. Kutt, D. P. Bybell, and R. VanBerg, IEEE Trans. Nucl. Sci. **NS-32**, 1429 (1985).

[30]P. H. Kutt and D. P. Balamuth, Comput. Phys. 52 (1989).

[31]F. Rybicki, T. Tamura, and G. R. Satchler, Nucl. Phys. **A146**, 659 (1970).

[32]R. R. Betts, private communication.

[33]R. J. Blin-Stoyle and M. A. Grace, in *Handbuch der Physik,* edited by S. Flügge (Springer, Berlin, 1957), Vol. 42, p. 555.

[34]A. Bohr, Nucl. Phys. **10**, 486 (1959).

[35]G. R. Satchler, *International Monographs on Physics* (Oxford University Press, New York, 1983), pp. 165–178.

[36]Y. Abe, J. Y. Park, K. Kato, S. Okabe, and T. Tazawa, in *Nuclear Physics with Heavy Ions,* Ref. 11.

[37]A. Mattis, W. Dünnweber, W. Trombik, A. Glaesner, D. Konnerth, and R. Ritzka, Phys. Lett. B **191**, 275 (1987).

[38]R. A. Broglia, C. H. Dasso, H. Esdensen, and A. Winther, Nucl. Phys. **A349**, 496 (1980).

[39]S. Cohen, F. Plasil, and W. Swiatecki, Ann. Phys. **82**, 406 (1974).

[40]R. Maass and W. Scheid, Phys. Lett. B **202**, 26 (1988).

[41]E. Uegaki and Y. Abe, Phys. Lett. B **231**, 28 (1989).